Design and Analysis of Linear Quadratic Gaussian Feedforward Controllers for Active Noise Control

Annea Barkefors, *Student Member, IEEE*, Mikael Sternad, *Senior Member, IEEE*, and Lars-Johan Brännmark

***Abstract*—A method for sound field control applied to active noise control is presented and evaluated. The method uses Linear Quadratic Gaussian (LQG) feedforward control to find a Minimal Mean Square Error (MMSE)-optimal linear sound field controller under a causality constraint. It is obtained by solving a polynomial matrix spectral factorization and a linear (Diophantine) polynomial matrix equation. An important component in the design is the control signal penalty term of the criterion. Its use and influence is here discussed and evaluated using measured room impulse responses. The results indicate that the use of a relatively simple, frequency-weighted penalty on individual control signals provides most of the benefits obtainable by the considered more advanced alternative. We also introduce and illustrate several tools for performance analysis. An analytical expression for the attainable performance clearly reveals the performance loss generated by having to use a causal controller instead of the ideal noncausal controller. This loss is largest at low frequencies. Furthermore, we introduce a measure of the reproducibility of the target noise sound field with given control loudspeaker setups and room transfer functions. It describes how well a controller that uses an input subspace of dimension equal to the effective rank of the system is able to reproduce a target sound field. This performance measure can e.g. be used to support the selection of good combinations of placements of control loudspeakers.**

***Index Terms*—Active noise reduction, sound field control, sound field reproducibility, effective rank, feedforward control, causality constraints, linear quadratic control.**

I. Introduction

A. Background

SOUND field control deals with the problem of controlling the acoustic field in a volume or area in space so that the controlled sound field approximates a predefined desired sound field. The goal can e.g. be equalization, to compensate for distortions introduced to a signal by the loudspeakers and room responses as in [1]–[3].

Manuscript received February 25, 2014; revised June 01, 2014; accepted August 02, 2014. Date of publication August 19, 2014; date of current version August 27, 2014. This work was supported in part by the Swedish Research Council under contract 2009-5527, by Dirac Research AB, and by the Knut and Alice Wallenberg foundation. The associate editor coordinating the review of this manuscript and approving it for publication was Prof. Woon-Seng Gan.

A. Barkefors and M. Sternad are with the Department of Engineering Sciences, Uppsala University, 751 21, Uppsala, Sweden, and also with Dirac Research AB, 753 23 Uppsala, Sweden (e-mail: annea.barkefors@signal.uu.se; mikael.sternad@signal.uu.se).

L.-J. Brännmark is with Dirac Research AB, 753 23 Uppsala, Sweden (e-mail: lars-johan.brannmark@dirac.se).

Color versions of one or more of the figures in this paper are available online at http://ieeexplore.ieee.org.

Digital Object Identifier 10.1109/TASLP.2014.2349856

One special case of sound field control is noise reduction, when silence in the controlled volume or area is desired. Then the desired sound field becomes the negative sound pressure deviation of the noise that is to be cancelled. Sound field control turns into active noise control, ANC.

Typically, traditional ANC systems use adaptive control algorithms [4]–[7]. While adaptive algorithms have the advantage of being flexible and able to follow changes in the characteristics of the noise, they are computationally demanding and may have stability problems. Also, there is a need for one or several microphones within the region of control.

In our work, we have focused on situations where the systems are linear and the surroundings are known not to change, or to change only between certain known states. Examples of this would be car compartments and airplane compartments. Then the transfer functions from available control loudspeakers to the volume of interest for control can be measured in advance, and a controller implemented offline. In the case when the conditions are known to change between certain known states, such as number of passengers in the car, one controller per state could be implemented and some gain scheduling scheme used. The reference signals to the controller (the measurable disturbances in a feedforward ANC problem) are assumed to have known first and second order moments. Under these assumptions, a model-based design of a Minimal Mean Square Error (MMSE)-optimal linear sound field controller can be obtained. Using a controller calculated offline in this way is less computationally demanding than using an adaptive scheme. There are examples of methods using fixed controllers, see for example [8] where low frequency road noise around 40 Hz is reduced in a consumer car, whereas most of the research on ANC in car compartments has been focused on adaptive techniques [9], [10].

Three main approaches to sound field control have been explored during the last decades, all of which suffer from important restrictions: Wave Field Synthesis [3], [11], [12] and High Order Ambisonics [13] are both mainly intended for audio reproduction. They are based on theoretical approximations of reality, which for ANC purposes is a major disadvantage. ANC demands high accuracy in the models that are being used, and theoretical approximations will never be detailed enough. Finally, we have multipoint Mean Square Error (MSE) designs, which are also in general performed as per-frequency designs [14], with some approaches using spherical harmonics [15], [16].

Here we investigate a multipoint MSE feedforward control strategy based on Linear Quadratic Gaussian (LQG) control that avoids these restrictions and that was recently proposed for use in feedforward ANC systems [17], [18]. This method utilizes

multiple loudspeakers to control the sound field within a target volume. It inherently takes the time-domain as well as the frequency-domain properties of the resulting sound field into account. An optimal stable controller in the form of IIR (Infinite Impulse Response) filters is obtained under specified constraints on transport delays and computational delays.

We use a polynomial equations approach to controller design [19]. Compared to state-space methods, the polynomial approach offers increased structural insight and also has good numerical properties. Compared to time domain matrix-based MSE methods for sound field control [20], the inversion of large block-Toeplitz matrices is avoided.

LQG feedforward control is relevant not only for ANC but also for other types of sound field control problems where multipoint MSE criteria are of interest. Recently the method has been applied successfully to problems of equalizer design and robust room compensation, see [2], [21]–[23], as well as to acoustical zone design [24].

B. Contributions

Three key issues are discussed in this paper. First, the use of model-based LQG feedforward control for ANC is outlined, including modeling aspects, design equations and expressions for the residual control errors and the minimal criterion value. The latter quantifies the performance loss incurred by a prescribed causality constraint.

Second, when we minimize a control-weighted MSE criterion, the properties of a frequency- and loudspeaker-dependent penalty on the control signals will determine the resulting performance. Constraints on the control loudspeaker powers have previously been introduced as simple scalar regularization terms [25] or Lagrange multipliers [26] in frequency-domain MMSE designs. The MIMO (Multiple Input Multiple Output) LQG design framework provides a much richer set of possibilities. The effects of different usages of the control signal penalty term in the criterion are investigated, both in terms of performance in relation to theoretical performance limits, and in terms of control signal energy usage.

Third, the theoretical concepts of the effective rank of the control path and the reproducibility of the desired sound field are evaluated as performance indicators and guidelines for loudspeaker placement. The loudspeaker placement problem has received increasing interest, with [27]–[29] proposing different optimization approaches for frequency-domain MMSE designs. In our case, we seek a tool that can assess the attainable performance of a given loudspeaker setup, taking into account the properties of a target sound field at multiple frequencies in a reverberant environment. The performance predictor is directly obtained from measured room transfer functions and it does not require the computationally demanding solution of the complete sound field control problem. These properties make it attractive to use in situations when a large number of loudspeaker designs, placements or other design elements are to be assessed and compared.

C. Outline of Paper

Section II discusses the sound field control problem and presents the design of an optimal feedforward LQG controller. The attainable performance is first expressed in terms of the minimal criterion value. Performance of the presented controller is then discussed in terms of the effective rank of the control path and the reproducibility of the desired sound field, i.e. how well the controller can reproduce the target sound field. Possible strategies for adjusting the control signal penalty matrix are then outlined. Section III presents an experimental evaluation based on measured room impulse responses. The usefulness of the effective rank and reproducibility measures are evaluated and the influence of different choices of time advance on the performance is shown. Further, the importance of investigating not only achieved levels of attenuation but also the remaining control error is illustrated. The influence of design choices and loudspeaker setup on the input signal economy is investigated and finally the effects outside the area of control are illustrated. A discussion and the conclusion is presented in Section IV.

D. Mathematical Notation and Some Terminology

The transpose of a matrix $\mathbf{M}$ is denoted $\mathbf{M}'$. Real-valued vectors $v(t)$ of discrete time signals are written in italics, as are scalars. Causal FIR (Finite Impulse Response)-filters with real-valued coefficients $\{p_n\}$ are represented by polynomials in the backward shift operator q^{-1}:

$$P(q^{-1}) = p_0 + p_1 q^{-1} + \cdots + p_{np} q^{-np}$$

For discrete-time shift operators, $v(t-1) = q^{-1}v(t)$ and $v(t+1) = qv(t)$. The time domain operator q^{-1} corresponds to z^{-1} or $e^{-j\omega}$ in the frequency domain, where ω is the normalized angular frequency. The frequency domain representation $|V(\omega)|^2$ of a discrete-time signal $v(t)$ refers to its power spectrum, i.e. the discrete Fourier transform of the autocorrelation function of $v(t)$. When the complex-valued frequency function $V(\omega)$ corresponds to a vector $v(t)$ of time-varying sound pressures, it is often denoted a complex sound field. Arguments of filters and system models will in some places be omitted where there is no risk of misunderstanding.

Polynomial matrices (matrices of FIR filters) are represented by bold italics, such as $\boldsymbol{M}(q^{-1})$ and rational matrices (matrices of rational discrete-time transfer functions) by bold calligraphic symbols, e.g. $\boldsymbol{\mathcal{H}}(q^{-1})$. Rational matrices are represented in terms of polynomial matrices by right matrix fraction descriptions (MFDs), $\boldsymbol{\mathcal{H}} = \boldsymbol{B}\boldsymbol{A}^{-1}$ [30].

A square polynomial matrix $\boldsymbol{M}(q^{-1})$ is said to be minimum phase if all zeros of $\det(\boldsymbol{M}(z^{-1}))$ are located within the unit circle $|z| < 1$ of the complex plane. All rational transfer functions in $\boldsymbol{M}^{-1}(q^{-1})$ are stable if $\boldsymbol{M}(q^{-1})$ is minimum phase. The conjugate matrix $\boldsymbol{M}_*(q)$ of a polynomial matrix $\boldsymbol{M}(q^{-1})$ with real-valued coefficients is defined as its transpose with the forward shift operator q substituted for q^{-1} as argument in all polynomials.

II. Linear Feedforward Sound Field Control

A. The Sound Field Control Problem

Our acoustic control system is modeled as linear and it utilizes N control loudspeakers to control the sound pressure field at M measurement positions (control points) in which the room

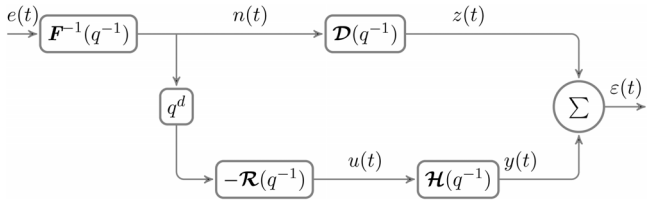

Fig. 1. Block diagram of the system, with noise path $\mathcal{D}(q^{-1})$, control path $\boldsymbol{\mathcal{H}}(q^{-1})$ and controller $\mathcal{R}(q^{-1})$. The model also includes an autoregressive process $\boldsymbol{F}^{-1}(q^{-1})$ to describe the spectral properties of the feedforward signals $n(t)$.

transfer functions have been measured. A block diagram of the discrete-time system is shown in Fig. 1. The transfer functions from the $N \times 1$ input vector $u(t)$ to the control loudspeakers to the $M \times 1$ output vector $y(t)$ at the measurement positions are described by a stable and causal right MFD of the form

$$y(t) = \boldsymbol{\mathcal{H}}(q^{-1})u(t) = \boldsymbol{B}(q^{-1})\boldsymbol{A}^{-1}(q^{-1})u(t), \qquad (1)$$

where all the delays are included in the models in the form of leading zero coefficients of the polynomial matrix $\boldsymbol{B}(q^{-1})$. This includes both transport delays and delays introduced by sound cards etc. Here, the polynomial matrices $\boldsymbol{B}(q^{-1})$ and $\boldsymbol{A}(q^{-1})$ have dimensions $M \times N$ and $N \times N$ respectively. When $\boldsymbol{A}(q^{-1}) = \mathbf{I}$, we have a set of FIR models. A physically motivated model structure is the use of (1) with $\boldsymbol{A}(q^{-1})$ being a diagonal polynomial matrix with equal diagonal elements, see section 2.7 of [21]. The roots of these filter polynomials would constitute common acoustic poles [31], representing the modes of the acoustic system. The transfer functions represented by $\boldsymbol{\mathcal{H}}(q^{-1})$ are variously called forward paths, secondary paths or control paths.

The primary paths from an $L \times 1$ vector $n(t)$ of measurable feedforward or reference signals to the M measurement positions are described by a second stable and causal discrete-time model in right MFD form:

$$z(t) = \mathcal{D}(q^{-1})n(t) = \boldsymbol{D}(q^{-1})\boldsymbol{E}^{-1}(q^{-1})n(t), \qquad (2)$$

where $\boldsymbol{D}(q^{-1})$ has dimensions $M \times L$ and $\boldsymbol{E}(q^{-1})$ has dimensions $L \times L$. Again, all the delays in the system are included as leading zero coefficients of the polynomial matrix $\boldsymbol{D}(q^{-1})$. In a feedforward ANC problem, $\mathcal{D}(q^{-1})$ would represent the noise path, and therefore be a part of the model of the controlled system. Specifically it would represent a model of the part of the total noise at each of the M control points that is perfectly correlated with at least some of the L noise measurement signals. Such linear models can be estimated by system identification [32], [33], based on measurements of $n(t)$ and of the resulting noise at the control points. Components of the noise that are uncorrelated with $n(t+\tau)$ for any τ cannot be damped by the feedforward controller and will therefore not have to be modeled.

In other sound field control applications, $\mathcal{D}(q^{-1})$ would represent the desired sound field response at the measurement positions. In such cases, it would constitute a part of the specification of the problem formulation.

The dynamic systems $\boldsymbol{\mathcal{H}}(q^{-1})$ and $\mathcal{D}(q^{-1})$ are here assumed to be linear, time-invariant and known. Their denominators, $\boldsymbol{A}(q^{-1})$ and $\boldsymbol{E}(q^{-1})$ are assumed to be monic, i.e. to have unit matrices as leading coefficient matrices, and to be minimum phase. Therefore their inverses are causal and stable rational matrices. The assumption that the primary path $\mathcal{D}(q^{-1})$ is known limits the applications for active noise control to situations where it is possible to model the primary path in advance.

The vector $n(t)$ is assumed to be available with a time advance of up to d samples. In sound field control with pre-recorded sound, a large advance q^d can sometimes be used. In ANC problems, this time advance represents the results of using a separate prediction of the reference signal $n(t)$. The signal $q^d n(t) = n(t+d)$ used below would in that case represent only the components of the measurement signals that are predictable by d samples[1]. Furthermore, $n(t)$ is assumed to have zero mean. Available knowledge of its second-order moments is represented here by a vector-autoregressive (AR) model

$$n(t) = \boldsymbol{F}^{-1}(q^{-1})e(t) \qquad (3)$$

where the $L \times L$ polynomial matrix $\boldsymbol{F}(q^{-1})$ is monic and where the $L \times 1$ vector $e(t)$ is white, with zero mean and known covariance matrix $E(e(t)e^T(t)) = \Lambda$. This part of the model will in many problems be nonstationary, and may have to be adjusted adaptively in real time. Lack of specific knowledge would be represented by a white noise model $n(t) = e(t)$. The attainable performance of the controller will depend on the properties of the dynamic systems $\mathcal{D}(q^{-1})$ and $\boldsymbol{\mathcal{H}}(q^{-1})$, the time advance d and the predictability of the feedforward signal $n(t)$, as specified by (3).

In the design process, the aim is to construct a rational linear and stable LQG feedforward controller $\mathcal{R}(q^{-1})$ that acts on the feedforward signal shifted d samples forward in time:

$$u(t) = -\mathcal{R}(q^{-1})n(t+d). \qquad (4)$$

The resulting feedforward control error is then

$$\begin{aligned}\varepsilon(t) &= z(t) + y(t) \\ &= (q^{-d}\mathcal{D}(q^{-1}) - \boldsymbol{\mathcal{H}}(q^{-1})\mathcal{R}(q^{-1}))n(t+d), \end{aligned} \qquad (5)$$

which is to be minimized. Thus, the linear controller $\mathcal{R}(q^{-1})$ is to be designed so that $\boldsymbol{\mathcal{H}}(q^{-1})\mathcal{R}(q^{-1})$ approximates the target path $q^{-d}\mathcal{D}(q^{-1})$ that includes a delay of d samples.

The performance of a linear causal feedforward controller (4) approaches that of a noncausal Wiener solution if $d \to \infty$, or if $n(t)$ is perfectly predictable over time. The latter case occurs if $n(t)$ is described by finite sums of sinusoids, which implies that the autoregressive model (3) has all poles (roots of $\det(\boldsymbol{F}(z^{-1}) = 0)$ on the unit circle $|z| = 1$. A noncausal Wiener design would correspond to an optimization of the controller $\mathcal{R}$ separately at each frequency of interest, without taking its time domain properties into account. See e.g. [25], [34] for such multipoint MMSE designs in the frequency domain.

[1]The LQG controller to be presented in Section II-B below contains an optimal (Wiener) predictor that appropriately utilizes the statistical knowledge of $n(t)$. However, it may in some problems be of advantage to use a separately designed predictor. We introduce the design variable d for this reason, and also to illustrate the noncausal limit, when $d \to \infty$.

B. Feedforward LQG Controller Design

Linear Quadratic Gaussian control uses the first and second order moments of the signal statistics to produce a linear controller that minimizes a quadratic criterion [35]. If all involved signals have Gaussian statistics, then the controller is optimal in the class of all linear and nonlinear controllers. This is the case here if $e(t)$ in (3) is Gaussian. If some signals are non-gaussian, then the controller is still optimal in the class of linear controllers.

The objective of the controller design is to minimize a scalar quadratic criterion representing the control-weighted MSE

$$J = E\{(\boldsymbol{V}(q^{-1})\varepsilon(t))'\boldsymbol{V}(q^{-1})\varepsilon(t) + (\boldsymbol{W}(q^{-1})u(t))'\boldsymbol{W}(q^{-1})u(t)\} \quad (6)$$

under constraints of stability and causality of $\mathcal{R}(q^{-1})$. The expectation $E\{\cdot\}$ in (6) is taken with respect to the statistics of $e(t)$ in (3).

The criterion (6) has two parts. The first penalizes a weighted sum of the control errors (5), and the $M \times M$ error penalty matrix $\boldsymbol{V}(q^{-1})$ may be used to give different weights on the errors in different spatial positions, at different frequencies or in different signal subspaces. In the second term, the $N \times N$ control signal penalty matrix $\boldsymbol{W}(q^{-1})$ influences the usage of the control loudspeakers. It can be used to prevent the loudspeakers from being used outside of their operating frequency ranges, as well as to direct the control signal energy into or away from certain directions in the control signal space. In noncausal Wiener solutions for multipoint MMSE designs, regularization often needs to be applied, see e.g. [25], [26]. A scalar regularization parameter $\alpha \geq 0$ would in our framework correspond to the use of $\boldsymbol{W} = \sqrt{\alpha}\mathbf{I}$. The design of $\boldsymbol{W}(q^{-1})$ will be discussed in more detail in Section II-E below. The noncausal case, for $d \to \infty$, is discussed in more detail in Section II-F.

The Optimal Controller: Assume that in the frequency domain, $\boldsymbol{W}_*(e^{j\omega})\boldsymbol{W}(e^{-j\omega})$ is positive definite for all frequencies ω. Then a unique stable linear feedforward controller (4) that minimizes the criterion (6) for the model (1), (2), (3), exists and is given by

$$\begin{aligned} u(t) &= -\mathcal{R}(q^{-1})n(t+d) \\ &= -\boldsymbol{A}(q^{-1})\boldsymbol{\beta}^{-1}(q^{-1})\boldsymbol{Q}(q^{-1})\boldsymbol{E}^{-1}(q^{-1})n(t+d), \end{aligned} \quad (7)$$

where the $N \times N$ causal and minimum phase polynomial matrix $\boldsymbol{\beta}(q^{-1})$, with causal and stable inverse, is obtained from the polynomial matrix spectral factorization (omitting arguments for brevity)

$$\boldsymbol{\beta}_*\boldsymbol{\beta} = \boldsymbol{B}_*\boldsymbol{V}_*\boldsymbol{V}\boldsymbol{B} + \boldsymbol{A}_*\boldsymbol{W}_*\boldsymbol{W}\boldsymbol{A} \quad (8)$$

or

$$\boldsymbol{A}_*^{-1}\boldsymbol{\beta}_*\boldsymbol{\beta}\boldsymbol{A}^{-1} = \boldsymbol{\mathcal{H}}_*\boldsymbol{V}_*\boldsymbol{V}\boldsymbol{\mathcal{H}} + \boldsymbol{W}_*\boldsymbol{W}, \quad (9)$$

and the $N \times L$ causal polynomial matrix $\boldsymbol{Q}(q^{-1})$ together with the $N \times L$ noncausal polynomial matrix $\boldsymbol{L}_*(q)$ are obtained as the unique solution to the polynomial matrix Diophantine equation

$$q^{-d}\boldsymbol{B}_*\boldsymbol{V}_*\boldsymbol{V}\boldsymbol{D} = \boldsymbol{\beta}_*\boldsymbol{Q} + q\boldsymbol{L}_*\boldsymbol{F}\boldsymbol{E}. \quad (10)$$

See Section 3.3 of [36] for a proof of optimality of the design equations (7)-(10), in a setting where (3) may be generalized to vector ARMA (Auto Regressive Moving Average) models.

Using the trace rotation rule, $\mathrm{tr}(\boldsymbol{AB}) = \mathrm{tr}(\boldsymbol{BA})$ and Parseval's formula, the scalar criterion value (6) can be expressed as

$$\begin{aligned} J = \mathrm{tr}\frac{1}{2\pi j}\oint_{|z|=1} &\left\{\boldsymbol{V}\left(z^{-d}\mathcal{D} - \boldsymbol{\mathcal{H}}\mathcal{R}\right)\boldsymbol{F}^{-1}\Lambda\boldsymbol{F}_*\right. \\ &\times \left(z^{d}\mathcal{D}_* - \mathcal{R}_*\boldsymbol{\mathcal{H}}_*\right)\boldsymbol{V}_* \\ &\left. + \boldsymbol{W}\mathcal{R}\boldsymbol{F}^{-1}\Lambda\boldsymbol{F}_*^{-1}\mathcal{R}_*\boldsymbol{W}_*\right\}\frac{dz}{z}. \end{aligned} \quad (11)$$

The individual diagonal elements of the two terms in the integrand of (11) reveal how the performance loss is influenced by the remaining noise powers in the M control points (first term) and by the control powers of the N elements of $u(t)$ (second term).

By using (1), (2), (3), trace rotation, the optimal controller expression (7) and the spectral factorization (8) in (11) and completing the squares, the minimal criterion value can be shown to be given by the following expression:

$$\begin{aligned} J_{min} = \mathrm{tr}\frac{1}{2\pi j}\oint_{|z|=1} &\boldsymbol{F}_*^{-1}\boldsymbol{E}_*^{-1}\boldsymbol{D}_*\boldsymbol{V}_*\left(\mathbf{I} - \boldsymbol{V}\boldsymbol{B}(\boldsymbol{\beta}_*\boldsymbol{\beta})^{-1}\boldsymbol{B}_*\boldsymbol{V}_*\right) \\ &\times \boldsymbol{V}\boldsymbol{D}\boldsymbol{E}^{-1}\boldsymbol{F}^{-1}\Lambda\frac{dz}{z} \\ + \mathrm{tr}\frac{1}{2\pi j}\oint_{|z|=1} &\boldsymbol{L}(\boldsymbol{\beta}_*\boldsymbol{\beta})^{-1}\boldsymbol{L}_*\Lambda\frac{dz}{z} \end{aligned} \quad (12)$$

It is shown in Appendix A that when $d \to \infty$, then $\boldsymbol{L}_*(q) \to 0$ in the Diophantine equation (10). Therefore, the first term in (12) represents the performance in the noncausal limit $d \to \infty$. The second term, which vanishes when $\boldsymbol{L}_* = 0$, represents the loss of performance caused by the causality constraint. This is further illustrated in Section III. The integrands of (12) can be studied in the frequency domain to reveal how these two terms vary with frequency.[2]

The polynomial feedforward controller design technique can be generalized to robust designs, that minimize the criterion on average over the model uncertainty [37]. Robustness with respect to the properties of the sound field in-between control points can be included [2], [21], [38]. The latter extension makes it possible to safely use the design at higher frequencies, above the spatial Nyquist frequency defined by the positioning of the M control points. However, in this paper we will not focus on the robust design extensions, but, in Section III, we will evaluate the design at frequencies below the spatial Nyquist frequency.

[2]Using the matrix inversion lemma and (8), the factor $\boldsymbol{I} - \boldsymbol{V}\boldsymbol{B}(\boldsymbol{\beta}_*\boldsymbol{\beta})^{-1}\boldsymbol{B}_*\boldsymbol{V}_*$ in (12) equals $(\boldsymbol{I} + \boldsymbol{B}\boldsymbol{V}(\boldsymbol{A}_*\boldsymbol{W}_*\boldsymbol{W}\boldsymbol{A})^{-1}\boldsymbol{B}_*\boldsymbol{V}_*)^{-1}$. If $\boldsymbol{W}(z^{-1})$ is positive definite for all $z^{-1} = e^{-j\omega}$, then this expression will be positive definite for all ω. Therefore, the integrand of the first term of (12) is a positive semidefinite $L \times L$-matrix at all frequencies.

Design procedure: To summarize a typical design procedure, appropriately placed control loudspeakers, with sufficient power in the frequency range must be available. A control path model (1) is estimated using test signals from these loudspeakers. Noise path models (2) are obtained from noise measurements. Solution of (8) and (10) then provide the controller (7), as an $N \times L$ matrix of IIR filters. The impulse responses of these filters can be approximated by long FIR filters, which in general provide less sensitivity to round-off errors.

A robust but lower-performance design can be obtained by assuming $n(t)$ to be white, i.e. by not taking its actual correlation properties into account. A higher performance design is obtained by adjusting a vector AR-model (3) to the statistics of $n(t)$. Changing noise statistics then must be tracked by adjusting this model and by periodically re-calculating the controller. When the AR-model (3) and/or the noise path model (2) change, while the secondary paths (1) stay constant, we only need to re-solve the Diophantine equation (10). The much more computationally demanding spectral factorization (8) remains constant. Such a strategy is one of indirect adaptive control [39]. It opens up the possibility of adaptation of high-order MIMO feedforward ANC systems to track time-varying properties of broadband as well as narrowband noise. The adaptive control potential of the proposed scheme is under current investigation [40].

C. The Frequency-Dependent Effective Rank of the Control Path

To understand the attainable performance of the controller introduced above, we need a characterization of the control path that describes the type of sound field it can create by using "reasonable" amounts of control energy.

Since the sound field that affects the criterion (6) via the error term is weighted by the error penalty matrix $\boldsymbol{V}(q^{-1})$ we will work here with the weighted room transfer functions $\boldsymbol{V}(q^{-1})\boldsymbol{\mathcal{H}}(q^{-1})$ and $\boldsymbol{V}(q^{-1})\mathcal{D}(q^{-1})$.

We now introduce a property of the weighted control path, the effective rank, that is a frequency-dependent measure. Therefore, the time domain operator q^{-1} is substituted by the frequency domain variable $e^{-j\omega}$ below.

The $M \times N$ matrix $\boldsymbol{V}(e^{-j\omega})\boldsymbol{\mathcal{H}}(e^{-j\omega})$ can be represented at frequency $\omega/2\pi$ by a singular value decomposition

$$\boldsymbol{V}\boldsymbol{\mathcal{H}} = \boldsymbol{\Psi}(\omega)\boldsymbol{\Sigma}(\omega)\boldsymbol{\Phi}^H(\omega) = \sum_{i=1}^{R} \sigma_i(\omega)\Psi_i(\omega)\Phi_i^H(\omega), \quad (13)$$

where $R = \min(M, N)$. The unitary matrices $\boldsymbol{\Psi}(\omega) = [\Psi_1(\omega) \dots \Psi_M(\omega)]$ of dimension $M \times M$ and $\boldsymbol{\Phi}(\omega) = [\Phi_1(\omega) \dots \Phi_N(\omega)]$ of dimension $N \times N$ contain the orthonormal left and right singular vectors of $\boldsymbol{V}(e^{-j\omega})\boldsymbol{\mathcal{H}}(e^{-j\omega})$ respectively. The real-valued scalar singular values $\sigma_1(\omega), \dots, \sigma_r(\omega)$, where $\sigma_i \geq \sigma_{i+1}$, are located on the diagonal of the otherwise zero $M \times N$ matrix $\boldsymbol{\Sigma}(\omega)$.

The left singular vectors $\{\Psi_i(\omega)\}$ are spatially sampled approximations to the Karhunen-Loève expansion functions (see e.g. Chapter 10.6 in [41]) of a continuous-space correlation function. Since $\boldsymbol{V}\boldsymbol{\mathcal{H}}$ has rank $\leq R = \min(M, N)$, at most R of the singular values are nonzero. These nonzero gains $\sigma_i(\omega)$ and corresponding left singular vectors $\Psi_i(\omega)$ are also denoted the *principal gains* and the *output principal directions* of the dynamic system [42]. Furthermore, some of the nonzero singular values may be insignificant. The frequency-dependent *effective rank* $r(\omega)$ can for the matrix $\boldsymbol{V}(e^{-j\omega})\boldsymbol{\mathcal{H}}(e^{-j\omega})$ be defined as

$$r(\omega) = \arg\min_r \left\{ \frac{\sum_{i=r+1}^{R} \sigma_i^2(\omega)}{\sum_{i=1}^{R} \sigma_i^2(\omega)} < \delta \right\}, \quad (14)$$

where $\delta = 0.001$ will be used throughout this paper. The effective rank is a discrete-space approximation of the essential dimensionality of a continuous-space sound field, also sometimes denoted the richness of the field, introduced in [43], [44].[3] The effective rank represents the number of significant principal gains of the control system at frequency $\omega/2\pi$. The subspace spanned by $\Phi_{r+1}(\omega), \dots, \Phi_N(\omega)$ represents the $(N - r)$-dimensional space of input principal directions that are "hard to use". Control signals that are sinusoids with frequency $\omega/2\pi$ would produce little acoustic output if they are scaled and phase-shifted so that they are a vector in this subspace. The subspace spanned by $\Psi_{r+1}(\omega), \cdots, \Psi_M(\omega)$ represents the $(M - r)$-dimensional space of output directions that are "hard to reach". Typically, the effective rank of the control paths increases with frequency and it increases linearly with the radius of a 2D area covered by the measurement positions [44].

D. Reproducibility of the Desired Sound Field

We now introduce a representation of how well a particular sound field can be approximated by the given setup. In particular, it characterizes how well the noise $n(t)$ can be controlled by a feedforward controller that uses only the components of the control paths represented by their effective rank. The target complex sound field, as seen by the criterion (6) via the error penalty matrix, $S(\omega) = \boldsymbol{V}(e^{-j\omega})Z(\omega) = \boldsymbol{V}(e^{-j\omega})\mathcal{D}(e^{-j\omega})N(\omega)$, is orthogonally projected onto the space spanned by $\Psi_1(\omega), \cdots, \Psi_r(\omega)$. The projection of $S(\omega)$ on $\Psi_m(\omega)$ is

$$\hat{S}_m(\omega) = \Psi_m(\omega)\Psi_m^H(\omega)S(\omega). \quad (15)$$

A summation over m, together with exchanging $S(\omega)$ for $\boldsymbol{V}(e^{-j\omega})\mathcal{D}(e^{-j\omega})N(\omega)$, gives the orthogonal projection as

$$\hat{S}(\omega) = \sum_{m=1}^{r} \Psi_m(\omega)\Psi_m^H(\omega)\boldsymbol{V}(e^{-j\omega})\mathcal{D}(e^{-j\omega})N(\omega). \quad (16)$$

The sound field $S(\omega) = \boldsymbol{V}(e^{-j\omega})\mathcal{D}(e^{-j\omega})N(\omega)$ can now be said to be reproducible by the weighted control paths

[3] A different definition of effective rank, based on an entropy-based measure of the singular values, has been introduced in [45].

$\boldsymbol{V}(e^{-j\omega})\boldsymbol{\mathcal{H}}(e^{-j\omega})$ at frequency $\omega/2\pi$ with relative error $\alpha(\omega)$, $0 \leq \alpha(\omega) \leq 1$, if

$$\frac{\|S(\omega) - \hat{S}(\omega)\|_2^2}{\|S(\omega)\|_2^2} \leq \alpha(\omega). \tag{17}$$

When $\alpha(\omega) = 0$, the target sound field is perfectly reproducible. At the other extreme, when $\alpha(\omega) = 1$, the target sound field lies in a subspace that cannot be reached by a control system that uses the part of the control paths defined by their effective rank at frequency $\omega/2\pi$.

It is shown in Section II-F below that under certain conditions, the frequency function (17) can be used to predict the performance of the controller (7), without actually having to design the controller. To investigate this property, we will in Section III compare the predicted relative error in dB, $-10\log_{10}(\alpha(\omega))$, to the error obtained by the controller (7).

A different method that has been suggested to predict attenuations in e.g. [10] is the multiple coherence function method. It gives the maximum attainable sound reduction as a function of frequency $\omega/2\pi$ as

$$\Delta(\omega) = -10\log\left(1 - \eta_{n:z}(\omega)\right), \tag{18}$$

where $\eta_{n:z}$ is the multiple coherence function between the feedforward signal $n(t)$ and the primary noise $z(t)$. This method therefore only takes the primary path into account. The reproducibility measure (17) will also incorporate information about the given control path and give the maximum attenuation that can be achieved for the combined system.

E. Designing the Control Signal Penalty Matrix

The control signal penalty matrix $\boldsymbol{W}(q^{-1})$ in (6) is used to influence the properties of the control loudspeaker inputs. It enables us to let physical constraints of the system that are not included in the linear model (1) to influence the criterion. Another way would be to introduce power limitations as hard constraints, an approach that is investigated for noncausal designs in e.g. [26] and [46]. Our method of instead allowing such side conditions to influence the design via criterion weights leads to simpler solutions than the latter approach.

Since $\boldsymbol{W}(q^{-1})$ appears in the spectral factorization equation (8) or (9) only via the term $\boldsymbol{W}_*(q)\boldsymbol{W}(q^{-1})$, the discussion and design outlined below is for $\boldsymbol{W}_*(q)\boldsymbol{W}(q^{-1})$ directly.

When comparing different designs that target different sets of control points, it is in some problems undesirable that the relation between the weighting of the error signals and the input signals in the criterion (6) should change depending on how many measurement positions are used. To prevent this, the penalty matrix $\boldsymbol{W}_*(q)\boldsymbol{W}(q^{-1})$ can be weighted by the number of measurement positions. Doing so will leave the balance in the criterion function between control power and error power per measurement position unchanged when changing the number M of measurement positions distributed over the area or volume to be controlled.

The design of the control signal penalty matrix will here be performed in two steps, addressing two different aspects of the control system. The matrix is thus subdivided additively into two terms,

$$\boldsymbol{W}_*(q)\boldsymbol{W}(q^{-1}) = \boldsymbol{W}_{1*}(q)\boldsymbol{W}_1(q^{-1}) + \boldsymbol{W}_{2*}(q)\boldsymbol{W}_2(q^{-1}). \tag{19}$$

The first and perhaps most apparent usage of the control signal penalty matrix is preventing the control loudspeakers from being used outside their operating frequency range. The matrix $\boldsymbol{W}_{1*}\boldsymbol{W}_1$ is used for this purpose. It can be chosen diagonal:

$$\boldsymbol{W}_{1*}\boldsymbol{W}_1 = \begin{bmatrix} W_{11*}W_{11} & 0 & \cdots & 0 \\ 0 & \ddots & & \vdots \\ \vdots & & \ddots & 0 \\ 0 & \cdots & 0 & W_{1N*}W_{1N} \end{bmatrix} \tag{20}$$

where each scalar FIR filter $W_{1j}(q^{-1})$ is designed in the frequency domain so that $W_{1j}(e^{-j\omega})$ has a small but nonzero gain in the operating frequency range of the corresponding loudspeaker, and a large gain outside of this range. Note that constructing $\boldsymbol{W}_{1*}(e^{j\omega})\boldsymbol{W}_1(e^{-j\omega})$ positive definite for all ω is a way to guarantee full rank of $\boldsymbol{\beta}_*(e^{j\omega})\boldsymbol{\beta}(e^{-j\omega})$ for all ω. This ensures that the spectral factor $\boldsymbol{\beta}$ from (8) is stably invertible, which is required in (7).

A second possible usage of the control signal penalty matrix is to prevent the controller from using the input principal directions that are hard to use, or equivalently, trying to affect output principal directions that are hard to reach with the current control loudspeaker setup, as discussed in Section II-C. If this subspace exists it is because one or several of the columns of $\boldsymbol{\mathcal{H}}(e^{-j\omega})$ are linearly dependent at frequency $\omega/2\pi$, or nearly linearly dependent. A linear dependence of the columns in $\boldsymbol{\mathcal{H}}(e^{-j\omega})$ might lead to numerical problems in the spectral factorization (9). Designing the control signal penalty matrix in the way described next will prevent such numerical problems.

Consider the rational spectral factorization (9), with the singular value decomposition (13) of its first right-hand term and the partitioning (19) of its last term:

$$\begin{aligned} \boldsymbol{A}_*^{-1}\boldsymbol{\beta}_*\boldsymbol{\beta}\boldsymbol{A}^{-1} &= \boldsymbol{\mathcal{H}}_*\boldsymbol{V}_*\boldsymbol{V}\boldsymbol{\mathcal{H}} + \boldsymbol{W}_*\boldsymbol{W} \\ &= \boldsymbol{\Phi}\boldsymbol{\Sigma}^H\boldsymbol{\Sigma}\boldsymbol{\Phi}^H + \boldsymbol{W}_{1*}\boldsymbol{W}_1 + \boldsymbol{W}_{2*}\boldsymbol{W}_2. \end{aligned} \tag{21}$$

Considered in the frequency domain, the $N \times N$ diagonal matrix $\boldsymbol{\Sigma}^H\boldsymbol{\Sigma}$ contains the R nonzero squared singular values $\{\sigma_i^2(\omega)\}$ along its diagonal. Among these, $\sigma_{r+1}^2(\omega) \ldots \sigma_R^2(\omega)$ are related to the hard-to-use input signal subspaces of the control path subsystem. If the penalty matrix $\boldsymbol{W}_{2*}\boldsymbol{W}_2$ is designed in the frequency domain such that

$$\boldsymbol{W}_{2*}(e^{j\omega})\boldsymbol{W}_2(e^{-j\omega}) = \boldsymbol{\Phi}(\omega)\mathbf{P}(\omega)\boldsymbol{\Phi}^H(\omega) \tag{22}$$

where

$$\mathbf{P}(\omega) = \begin{bmatrix} 0 & 0 & \cdots & & & \cdots & 0 \\ 0 & \ddots & & & & & \vdots \\ \vdots & & 0 & & & & \\ & & & \rho_{r+1}(\omega) & & & \vdots \\ \vdots & & & & & \ddots & 0 \\ 0 & \cdots & & & \cdots & 0 & \rho_N(\omega) \end{bmatrix}, \tag{23}$$

then the real-valued scalar penalty terms $\{\rho_i\}$ could be used to penalize exactly the part of the control power that will go into this subspace. By setting the ρ_i s large, this "unnecessary" part of the control energy could be eliminated. Quantitative guidelines on the choice of penalties and their relations to the singular values of the control paths are derived next.

F. Connection Between the Measure of Reproducibility and the Control Signal Penalty Matrix

We return to the singular value decomposition (13) and will focus here on the limiting case of the noncausal controller, i.e. the case $d \to \infty$. This would in practice apply to cases with narrowband noise, which is predictable so that a prediction can generate $n(t+d)$ for large d. The design is performed under the assumption that the control penalty matrix $\boldsymbol{W}_*(e^{j\omega})\boldsymbol{W}(e^{-j\omega})$ is designed as

$$\boldsymbol{W}_*\boldsymbol{W} = \boldsymbol{W}_{2*}\boldsymbol{W}_2 = \boldsymbol{\Phi}\boldsymbol{\Sigma}_\rho^2\boldsymbol{\Phi}^H, \tag{24}$$

where $\boldsymbol{\Sigma}_\rho^2(\omega) = \operatorname{diag}(\rho_i(\omega)), i = 1 \ldots N$. Note that so far this is a generalization of the design (22) of $\boldsymbol{W}_{2*}(e^{j\omega})\boldsymbol{W}_2(e^{-j\omega})$ that was introduced in the previous section.

The noncausal limiting Wiener solution to the LQG feedforward control problem is expressed as a rational matrix $\mathcal{R}(q, q^{-1})$ with double-sided infinite impulse response. It is obtained as the limit

$$\mathcal{R}_{nc}(q, q^{-1}) = \lim_{d\to\infty} \mathcal{R}(q^{-1})q^d \tag{25}$$

of the causal solution. Since $\boldsymbol{L}_*(q) \to 0$ in the Diophantine equation (10) when $d \to \infty$ (see Appendix A), the Diophantine equation (10) in the noncausal limit approaches the identity

$$q^{-d}\boldsymbol{B}_*(q)\boldsymbol{V}_*(q)\boldsymbol{V}(q^{-1})\boldsymbol{D}(q^{-1}) = \boldsymbol{\beta}_*(q)\boldsymbol{Q}(q^{-1}). \tag{26}$$

The limiting expression $\boldsymbol{Q}_{nc}(q^{-1}) = \lim_{d\to\infty}\boldsymbol{Q}(q^{-1})$ for the polynomial matrix $\boldsymbol{Q}(q^{-1})$ is therefore given by

$$\boldsymbol{Q}_{nc} = \lim_{d\to\infty} q^{-d}\boldsymbol{\beta}_*^{-1}\boldsymbol{B}_*\boldsymbol{V}_*\boldsymbol{V}\boldsymbol{D}. \tag{27}$$

Inserting this expression for $\boldsymbol{Q}_{nc}(q^{-1})$ into (7), the corresponding limiting frequency domain expression for the control signal from the noncausal controller $\mathcal{R}_{nc}(e^{-j\omega}) = \lim_{d\to\infty}\mathcal{R}e^{j\omega d}$ becomes

$$\begin{aligned} U(\omega) &= -\mathcal{R}_{nc}N(\omega) = \lim_{d\to\infty} -\boldsymbol{A}\boldsymbol{\beta}^{-1}\boldsymbol{Q}\boldsymbol{E}^{-1}e^{j\omega d}N(\omega) \\ &= -(\boldsymbol{A}_*^{-1}\boldsymbol{\beta}_*\boldsymbol{\beta}\boldsymbol{A}^{-1})^{-1}\boldsymbol{\mathcal{H}}_*\boldsymbol{V}_*\boldsymbol{V}\mathcal{D}N(\omega). \end{aligned} \tag{28}$$

Now the singular value decomposition (13) can be used together with (21) and (24) for the control signal penalty matrix to express the noncausal controller as

$$\begin{aligned} \mathcal{R}_{nc} &= \left(\boldsymbol{\Phi}(\boldsymbol{\Sigma}^H\boldsymbol{\Sigma} + \boldsymbol{\Sigma}_\rho^2)\boldsymbol{\Phi}^H\right)^{-1}\boldsymbol{\Phi}\boldsymbol{\Sigma}^H\boldsymbol{\Psi}^H\boldsymbol{V}\mathcal{D} \\ &= \boldsymbol{\Phi}\operatorname{diag}\left(\frac{\sigma_i}{\sigma_i^2+\rho_i}\right)\boldsymbol{\Psi}^H\boldsymbol{V}\mathcal{D}, \end{aligned} \tag{29}$$

since $\boldsymbol{\Phi}^H = \boldsymbol{\Phi}^{-1}$. The matrix $\operatorname{diag}(\cdot)$ has dimension $N \times M$.

The effect of the control signal on the resulting sound field at frequency ω, weighted by the error penalty matrix $\boldsymbol{V}(e^{-j\omega})$, becomes

$$\begin{aligned} \boldsymbol{V}\boldsymbol{\mathcal{H}}\mathcal{R}_{nc}N(\omega) &= \boldsymbol{\Psi}\Sigma\boldsymbol{\Phi}^H\boldsymbol{\Phi}\operatorname{diag}\left(\frac{\sigma_i}{\sigma_i^2+\rho_i}\right)\boldsymbol{\Psi}^H\boldsymbol{V}\mathcal{D}N(\omega) \\ &= \boldsymbol{\Psi}\operatorname{diag}\left(\frac{\sigma_i^2}{\sigma_i^2+\rho_i}\right)\boldsymbol{\Psi}^H\boldsymbol{V}\mathcal{D}N(\omega) \\ &= \sum_{i=1}^{N}\left(\frac{\sigma_i^2}{\sigma_i^2+\rho_i}\right)\Psi_i\Psi_i^H\boldsymbol{V}\mathcal{D}N(\omega), \end{aligned} \tag{30}$$

where $\Psi_i(\omega)$, $i = 1 \ldots N$ are the N first left singular vectors of $\boldsymbol{V}(e^{-j\omega})\boldsymbol{\mathcal{H}}(e^{-j\omega})$. If the penalty weights $\rho_i(\omega)$ in (24) are chosen, as suggested by (23) in the previous section, such that $\rho_i(\omega) = 0$, $i = 1 \ldots r$ and if we furthermore set

$$\rho_i(\omega) \gg \sigma_i^2(\omega), \quad i = r+1, \ldots, N \tag{31}$$

we obtain

$$\begin{aligned} \boldsymbol{V}\boldsymbol{\mathcal{H}}\mathcal{R}_{nc}N(\omega) &= \sum_{i=1}^{r}\Psi_i\Psi_i^H\boldsymbol{V}\mathcal{D}N(\omega) \\ &\quad + \sum_{i=r+1}^{N}\left(\frac{\sigma_i^2}{\sigma_i^2+\rho_i}\right)\Psi_i\Psi_i^H\boldsymbol{V}\mathcal{D}N(\omega) \approx \hat{S}(\omega), \end{aligned} \tag{32}$$

where $\hat{S}(\omega)$ was defined in (16). This leaves the total weighted error

$$\lim_{d\to\infty}\boldsymbol{V}\mathcal{E}(\omega) = \left(\boldsymbol{V}\mathcal{D} - \boldsymbol{V}\boldsymbol{\mathcal{H}}\mathcal{R}_{nc}\right)N(\omega) \approx S(\omega) - \hat{S}(\omega). \tag{33}$$

In other words, when designing the control signal penalty matrix as outlined by (22)–(23) and using much larger penalty weights in (23) than the corresponding squared singular values of the weighted control path (13) at that frequency, the performance of the feedforward controller should in the noncausal limit be close to that predicted by the reproducibility measure (17) introduced in section II-D.

III. Experiments

Several experiments were performed to investigate the performance of the feedforward controller applied for noise cancellation in a setup described by Fig. 2.

Before the experiments, the models $\mathcal{D}(q^{-1})$ and $\boldsymbol{\mathcal{H}}(q^{-1})$ in Fig. 1 needed to be identified. In the identification process, high order FIR models have been used. Therefore, $\boldsymbol{A}(q^{-1}) = \mathbf{I}$ in (1) and $\boldsymbol{E}(q^{-1}) = \mathbf{I}$ in (2). The identifications were made using swept sinusoids as excitation signals. The controllers were designed as IIR filters according to (7). Here we approximated them using high order FIR filters, which provides a simple and safe design with respect to numerical rounding errors.[4]

All measurements were performed with a sampling frequency of 44.1 kHz. However, since the frequencies of interest

[4]Implementation as IIR filters provides lower numerical complexity, but care must be taken with respect to the filter realization and its sensitivity to rounding errors.

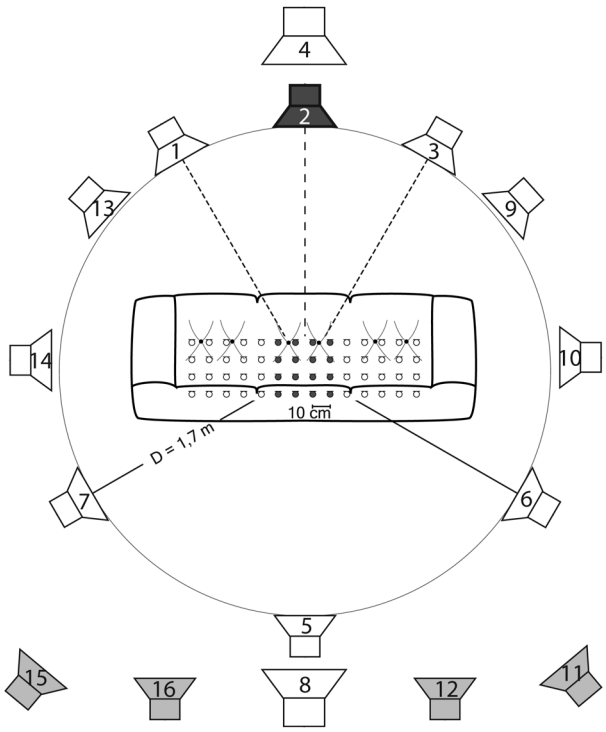

Fig. 2. The experimental setup. There are 14 midrange loudspeakers and two subwoofers (drawn as larger loudspeaker symbols) placed around a living room sofa. The loudspeaker that is marked dark gray is used as noise source in the experiments. Above the sofa there are 224 measurement positions distributed over a volume of $1.3 \times 0.3 \times 0.3$ m. The measurement positions are marked by '◯' symbols. The 16 measurement positions marked gray are called Grid 1, which is placed at ear height and covers an area of 0.3×0.3 m in the xy-plane.

TABLE I
THE HEIGHTS OF LOUDSPEAKERS SET UP AROUND A LIVING ROOM SOFA ACCORDING TO FIG. 2

Speaker number	Height [m]	Speaker Number	Height [m]
1	1.15	9	1.75
2	1.15	10	1.45
3	1.15	11	1.8
4	0.4	12	1.15
5	1.95	13	1.75
6	1.25	14	1.45
7	1.25	15	1.8
8	0.4	16	1.25

are below 1000 Hz, the data has been downsampled by a factor 10 before processing in order to reduce the computational burden.

A. Experimental Setup

All experiments were performed in a room of dimensions 4.6 m $\times$ 6 m $\times$ 2.6 m, furnished to have similar acoustic properties as those of a living room. As is shown in Fig. 2, 16 loudspeakers, of which two were subwoofers and 14 midrange, were placed at different heights, see Table I, around a living room sofa. The impulse responses from all loudspeakers to 224 measurement positions above the sofa were measured using two microphones. The measurement positions were spaced $d_m = 0.1$ m apart and spanned a volume of 1.3 m $\times$ 0.3 m $\times$ 0.3 m.

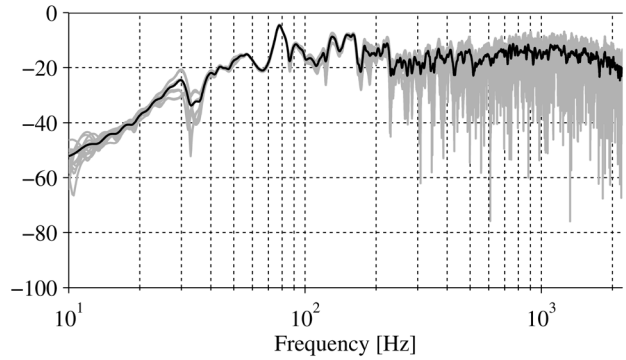

Fig. 3. Frequency response in dB of the noise speaker (speaker 2) to Grid 1. The gray curves show the individual responses to the 16 measurement positions, and the black curve shows their rms average.

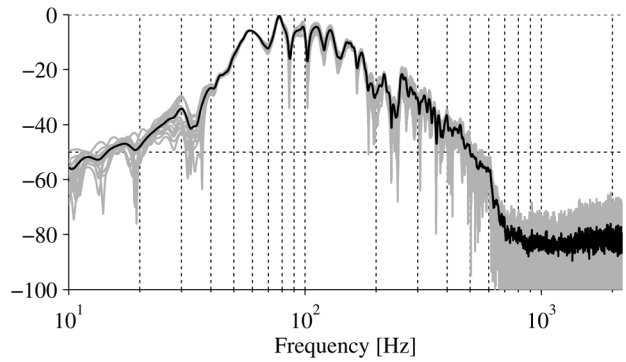

Fig. 4. Frequency response in dB of one of the subwoofers (speaker 4) to Grid 1. The gray curves show the individual responses to the 16 measurement positions, and the black curve shows their rms average.

From this measurement grid, a smaller grid has been selected, with 16 measurement positions that span an area of 0.3 m $\times$ 0.3 m in the xy-plane at ear height. This grid is marked by dark gray in Fig. 2 and will be referred to in the following as Grid 1. This is the area that is chosen for control.

From the closest loudspeaker, the distance to the center of the measured volume was 1.7 m, which makes the nearfield components of the sound field negligible. Therefore, the spatial Nyquist frequency for this setup becomes $f_N = c/2d_m = 344/0.2 = 1720$ Hz, where c is the speed of sound. This frequency lies well above the frequencies of interest for ANC.[5]

One loudspeaker was selected to act as noise source in the experiments. This loudspeaker, numbered 2 and colored dark gray in Fig. 2, will be referred to as noise source or noise speaker below. The magnitude responses of the noise paths or target paths, from the noise source to the measurement positions in Grid 1, are shown in Fig. 3, together with their rms average. The frequency responses of the other midrange loudspeakers are similar, though they will differ due to the different placements in the room. In Fig. 4 the magnitude responses from one of the subwoofers to the same 16 measurement positions are shown, again together with their rms average, to indicate the difference in frequency range for the subwoofers compared to the midrange loudspeakers.

[5]Also when taking some nearfield phenomena into account, and therefore using Kirkeby's rule of thumb [34] to have three measurement positions per wavelength, the highest frequency that is usable is still rather high for ANC purposes; 1147 Hz.

B. Design Choices

1) Modeling Delay, or Time Advance: The feedforward reference signal time advance, which corresponds to a delay in the noise path, is set to $d = 441$ samples, corresponding to 0.1 s. This gives a controller with performance close to, but somewhat below that of the noncausal limiting case. In Section III-D, a controller is designed also for the modeling delay $d = 0$, to highlight the difference in performance.

2) Error Penalty Matrix: The objective here is to perform ANC in the entire area in space corresponding to Grid 1 and no measurement position is more important than any other. The choice for the error penalty matrix is therefore $\boldsymbol{V}(q^{-1}) = \mathbf{I}$.

3) Control Signal Penalty Matrix: The impact on the control signal energy levels of using various control signal penalty matrix designs will be investigated in Section III-F. For the other experiments, we use the simple frequency-weighted diagonal matrix $\boldsymbol{W}_1(q^{-1})$ designed as described in Section II-E, setting $\boldsymbol{W}_2(q^{-1}) = 0$ in (19). Each diagonal element of $\boldsymbol{W}_{1*}\boldsymbol{W}_1$ is designed in the frequency domain to have a low gain (-25 dB) within the operating frequency region of the corresponding control loudspeaker and a high gain (0 dB) outside of it. The operating frequency region of the midrange loudspeakers is chosen from inspection of Fig. 3 to be 40 Hz to 1500 Hz, where the upper limit defines the control bandwidth and is set close to the spatial Nyquist frequency of the measurement grid. For the subwoofers, the operating frequency region is selected as 30–400 Hz, see Fig. 4. Finally, the elements of $\boldsymbol{W}_{1*}\boldsymbol{W}_1$ have been weighted with the number M of measurement positions as discussed in Section II-E.

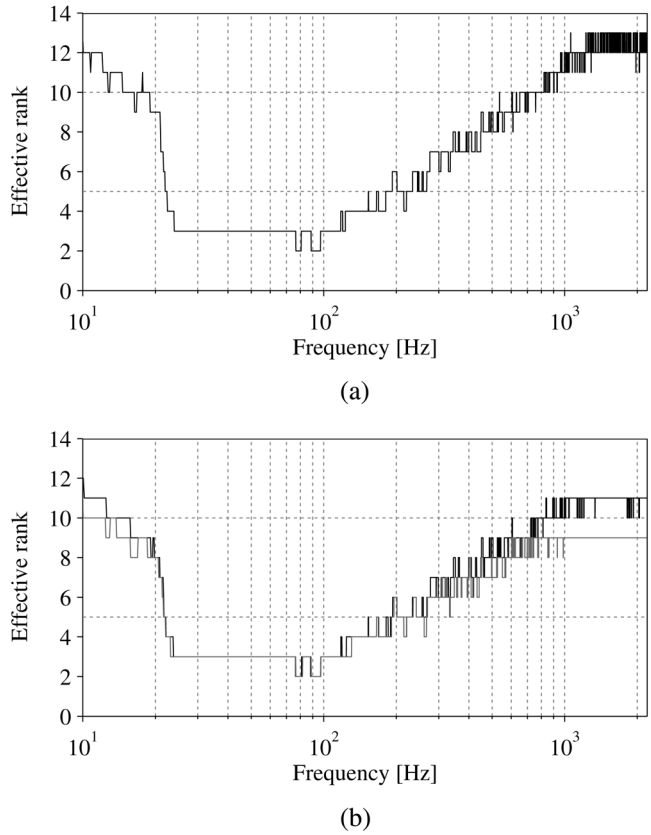

Fig. 5. The effective rank of the control system in Grid 1 using three different loudspeaker setups (a) The effective rank using 15 control loudspeakers (b) The effective rank using 13 control loudspeakers (black curve) and 11 control loudspeakers (gray curve).

C. Influence of the Effective Rank

This subsection illustrates how the effective rank and the measure of reproducibility can be used to investigate if the number of loudspeakers used for control can be reduced without appreciably affecting the obtainable attenuation. Grid 1 is used as the target area.

In Fig. 5(a) the effective rank of the control path as defined by (14) is shown, using all 15 control loudspeakers. The effective rank increases with frequency, which can be expected since the complexity of a sound field will increase with frequency. The effective rank for this model also increases for frequencies below 30 Hz, an effect that is caused by model errors due to low signal amplitudes and noise in the measurements.

Going back to the higher frequencies, Fig 5(a) shows that the maximum effective rank is 13. Considering that 15 loudspeakers are used, of which only the 13 midrange speakers produce significant power above 400 Hz, the theoretical limit for the effective rank is 13. In other words, for frequencies above 1200 Hz, where the effective rank saturates, all available midrange control loudspeakers would be needed. However, for ANC purposes, the frequencies of interest lie below 1200 Hz. It might for example be possible to remove two loudspeakers without affecting the effective rank of the system for frequencies up to 900 Hz. Up to four loudspeakers could be removed if accepting the highest frequency to drop to 600 Hz. How to choose which loudspeakers to remove is not obvious from the singular value decomposition but the geometry of the setup can often give some hints as to which loudspeaker positions may be superfluous. For the given setup the two loudspeakers number 11 and 15 that are marked light gray in Fig. 2 could be removed, or if four loudspeakers are to be removed, also number 12 and 16 since they contribute from spatial directions close to those of some of the other control loudspeakers. They are also the furthest away from the region of interest for control. Fig. 5(b) shows the effective rank for the system both after removing two and four loudspeakers as described.

A comparison of the effective rank for 15 loudspeakers and for 13 shows that there is very little difference for frequencies up to 900 Hz. Above 900 Hz, the original system has higher effective rank, as expected. Comparing with the effective rank for the system when using only 11 loudspeakers shows that the effective rank is still very similar up to around 400 Hz but then it drops somewhat compared to the two other systems of 13 and 15 loudspeakers.

The effective rank is an integer quantity. As the effective rank increases, the number of principal gains being summed in (14) increases as well, but the relative contribution of each added principal gain decreases. This means that the effective rank becomes more sensitive to small changes in the principal gains, leading to the oscillatory behavior in Fig. 5.

Next, the reproducibility of the target sound field by the control system is calculated, both for the initial system of 15 control loudspeakers and for the reduced systems. The results are shown in Fig. 6. The reproducibility measure α defined by (17)

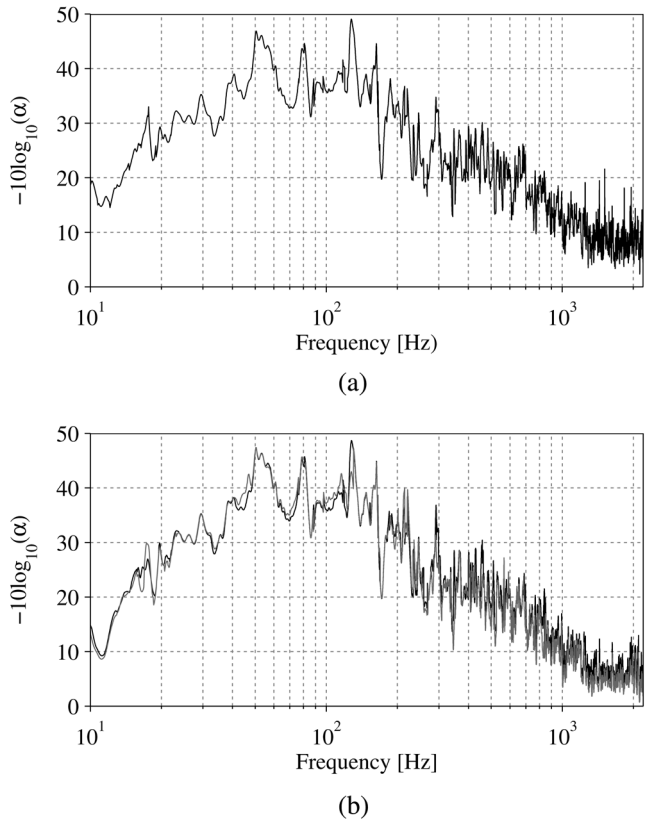

Fig. 6. The reproducibility in Grid 1 of the target sound field by the control sound field using three different loudspeaker setups (a) Reproducibility of the target using 15 control loudspeakers (b) Reproducibility of the target using 13 control loudspeakers (black curve) and 11 control loudspeakers (gray curve).

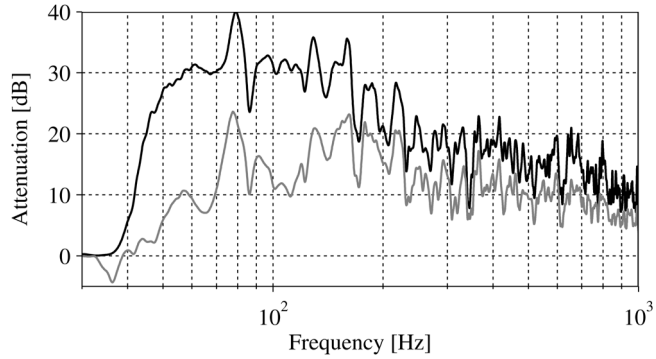

Fig. 7. The rms average attenuation in Grid 1 of a controller calculated for 11 control loudspeakers with $d = 441$ samples (black curve), and a controller calculated for 11 control loudspeakers and $d = 0$ (gray curve).

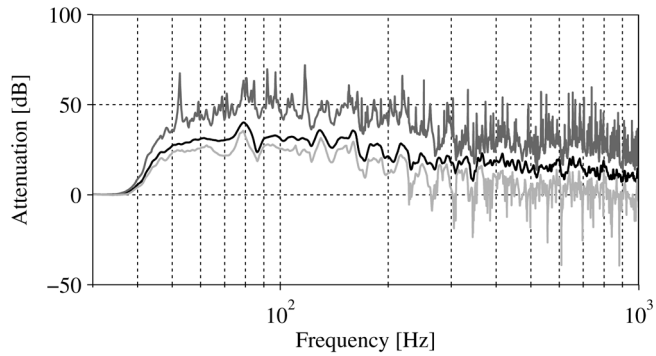

Fig. 8. The rms average of the attenuation (black curve) over Grid 1 after control, together with the maximum (dark gray curve) and minimum (light gray curve) attenuation. 11 control loudspeakers are used.

is plotted as $-10\log(\alpha)$, to give a correspondence to the possible achievable power attenuation. A high reproducibility is predicted, with possible achievable attenuations above 20 dB for 15–350 Hz. There are small differences in the reproducibility for the three systems up to 1200 Hz. Even for frequencies where the system of 15 control loudspeakers had a higher effective rank than the reduced systems, the differences in reproducibility are small.

Two comments on reproducibility: In the example above, $n(t)$ was selected scalar and white and corresponds to the input signal to the single noise source. In general, we may have dimension $L > 1$ for $n(t)$ and nonstationary situations, e.g. with multiple noise sources coming from time-varying directions. The measure (17) can then still be used, but will have to represent a set of curves that span the range of possibilities.

Furthermore, note that the noise $z(t)$ has in (2) been defined as the component of the noise at the control points that can be modeled by a linear dynamic system (2) with $n(t)$ as input. The reproducibility measure describes the reproducibility of this component only. The total noise may in addition have significant components that are uncorrelated with $n(t)$.

D. Influence of the Time Advance d

As we have shown in Section II-B, the performance of the controller can be divided into two terms as in (12). The second term of (12) represents the loss of performance caused by the causality constraint. The feedforward reference signal time advance has a direct influence on this term. This is illustrated in Fig. 7 which shows the attainable attenuations for two controllers implemented for the control system consisting of the 11 control loudspeakers marked white in Fig. 2. The first controller (black curve) is implemented with time advance $d = 441$ samples, and the second with $d = 0$ samples. The figure shows that it is mainly in the lower frequencies that the change of d has an impact on the performance. We have found a similar pattern also in experiments in a car cabin [18].

E. Variability of the Attenuation and Remaining Control Error over the Control Points

The maximum, minimum and rms average attenuation over Grid 1 is shown in Fig. 8 for a design made with 11 control loudspeakers, evaluated for the measured transfer functions. The controller of Section II-B was used, using a time advance $d = 441$ samples, corresponding to 0.1 s, error penalty matrix $\boldsymbol{V}(q^{-1}) = \mathbf{I}$ and control penalty matrix $\boldsymbol{W}(q^{-1}) = \boldsymbol{W}_1(q^{-1})$ as described in Section III-B.

It can be noted that the rms average of the simulated attenuation over the 16 measurement points (black curve in Fig. 8) follows the reproducibility curve for 11 loudspeakers in Fig. 6b rather well, although the control penalty ($\boldsymbol{W} = \boldsymbol{W}_1$) was not designed with this property in mind. This aspect will be discussed more extensively in Section III-F below.

There are several frequencies for which the minimum attenuation in Fig. 8 is negative by over 20 dB. Noise at these frequencies is in other words greatly amplified in at least one position within the grid. To understand why the controller is allowed to

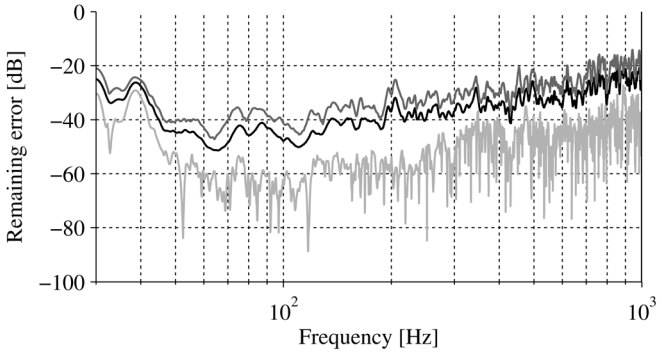

Fig. 9. The remaining noise after control over Grid 1. The black curve represents the rms average of the control error $E|\mathcal{E}(\omega)|^2$, the dark gray curve the maximum value and the light gray curve the minimum value over all 16 control points within Grid 1.

cause such amplifications, we need to inspect the target transfer function, that from the noise speaker, shown in Fig. 3. There are many deep but very narrow dips in amplitude for individual measurement positions for frequencies above 200 Hz. The frequencies with high noise amplification coincide with these dips. The sound pressure level is very low in such a dip, and therefore the resulting sound pressure level after control remains low even if it has been amplified by up to 20 dB.

The criterion (6) targets the sum of the squared errors and not the attenuation. Therefore it makes sense to inspect not only the obtained attenuation but also the remaining error. Fig. 9 shows the rms average remaining error $E|\mathcal{E}(\omega)|^2$ together with the maximum and minimum error over Grid 1 after control. It shows that what looks from Fig. 8 to be a disastrous amplification of the noise turns out to have limited effects. The maximum error curve is smooth with no huge remaining error for any frequency as compared to the other frequencies or measurement positions.

As an illustration, time plots from a simulated attenuation of a noise signal containing energy in a narrow frequency band around 150 Hz are shown in Fig. 10. The noise $n(t)$ was created by running white noise through an AR process with one pole pair placed with radius = 0.99 at 150 Hz. The original noise $z(t)$ is shown together with the remaining error $\varepsilon_i(t)$ for the measurement position i with the minimum attenuation, 26.8 dB in Fig. 10a, and in Fig. 10b for the measurement position with maximum attenuation, 40.1 dB.

F. Control Signal Economy

It is now investigated to what extent the number of utilized loudspeakers and also the total control input power can be reduced without appreciably affecting the control performance. We also investigate the effectiveness of penalizing the use of hard-to-use control input directions. Three designs are made for Grid 1. The choices of modeling delay d and the error penalty matrix $\boldsymbol{V}(q^{-1})$ are selected as discussed in section III-B, namely d corresponding to 0.1 s and $\boldsymbol{V}(q^{-1}) = \mathbf{I}$.

Case 1: A controller is designed to use all 15 available control loudspeakers. The control signal penalty matrix $\boldsymbol{W}(q^{-1})$ is here chosen diagonal, using $\boldsymbol{W}_1(q^{-1})$ as described in Section III-B3.

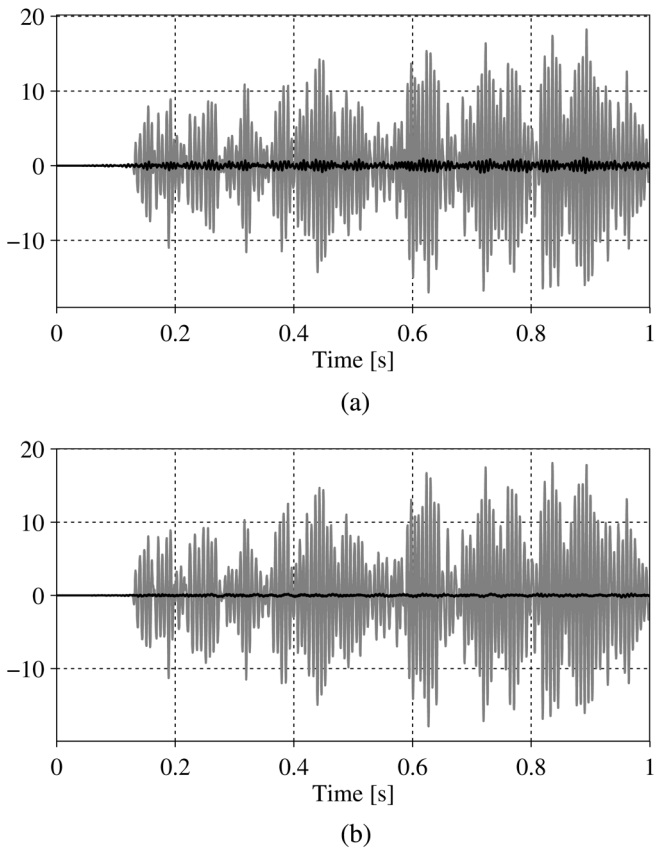

Fig. 10. Time plots showing the measurement positions with the lowest and the highest attenuation of a noise signal. The gray curves show the original noise signal and the black curves show the remaining error after control (a) Minimum attenuation over the grid, 26.8 dB (b) Maximum attenuation over the grid, 40.1 dB.

Case 2: Four of the control loudspeakers are removed, in the same way as in section III-C, leaving a control system consisting of 11 control loudspeakers, which are marked white in Fig. 2. The control signal penalty matrix $\boldsymbol{W}(q^{-1})$ is chosen in the same way as for *Case 1*. One advantage of removing control loudspeakers is of course that there is a cost of using hardware that is not essentially needed. It is also interesting to see how removing loudspeakers in this way influences the use of control power by the remaining loudspeakers. Will the power that in *Case 1* is sent to the four removed loudspeakers merely be redistributed over the remaining control loudspeakers or will the total power be reduced?

Case 3: The same control system with 11 loudspeakers is used as in *Case 2*, but the control signal penalty matrix $\boldsymbol{W}(q^{-1})$ is designed as described in Section II-D, with $\boldsymbol{W}_{1*}\boldsymbol{W}_1$ being the same as in *Case 2*, and the term $\boldsymbol{W}_{2*}\boldsymbol{W}_2$ by (22) added. The penalties $\{\rho_{r+1}(\omega) \dots \rho_{11}(\omega)\}$ in (17) are chosen as $\rho_i = \sigma_r^2$, $i = r+1, \dots, 11$, which implies that $\rho_i \gg \sigma_i^2$ for $i = r+1, \dots, N$, fulfilling condition (31). This case was investigated to find out if penalizing the nullspace in the way described would be of advantage.

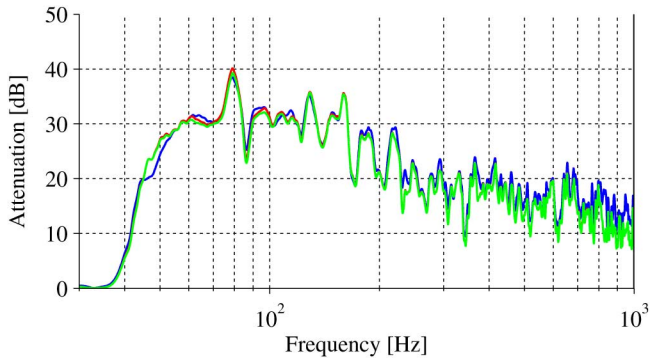

Fig. 11. Simulated attenuation of the noise. The blue curve represents the average attenuation achieved in Grid 1 using 15 control loudspeakers and a flat diagonal control signal penalty matrix, and the red curve using the same type of control signal penalty matrix design, but only 11 control loudspeakers. The green curve represents the average attenuation when 11 control loudspeakers are used together with an control signal penalty matrix designed from the nullspace of the control system. The curves are difficult to distinguish, so the difference between the red and the green curve is shown for clarity in Fig. 12.

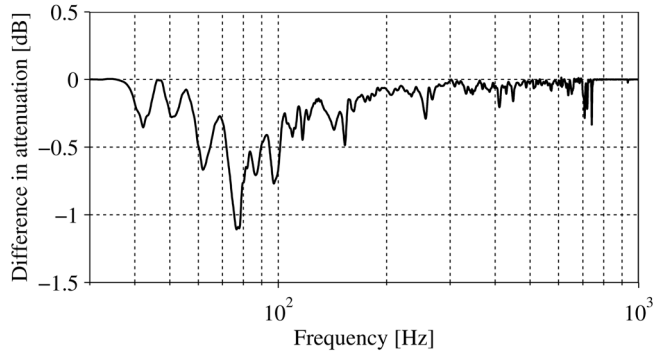

Fig. 12. Difference in achieved attenuation between using a simple diagonal control signal penalty matrix and a control signal penalty matrix designed from the nullspace of the control system. In both cases, 11 control loudspeakers were used.

Simulated attenuation curves were created, showing in Fig. 11 the rms average over Grid 1 for all three cases. It can be seen from the figure that going from *Case 1* to *Case 2* or *3* gives no severe degradation of the average performance over Grid 1 for any frequency band up to 1000 Hz.

The green curve in Fig. 11 (rms average for 11 loudspeakers according to *Case 3*) can be compared to the corresponding reproducibility curve in Fig. 6(b). According to the discussion in Section II-F, the performance of the controller designed for *Case 3* is predicted by the reproducibility curve, if the time advance d is chosen large enough for the controller to approach the noncausal solution and if the scalar penalties $\{\rho_i\}$ of (23) are chosen sufficiently large. A comparison between the two figures shows that the resulting attenuation follows the general trend of the reproducibility curve, but in particular for frequencies below 180 Hz, the obtained attenuation is lower than predicted. The most likely cause for the difference is our use of a large but still finite time advance d, whereas the reproducibility results hold for $d \to \infty$. In Fig. 7, and also in [47], it was found that the impact of the time advance is mainly in the lower frequencies, resulting in worse agreement with the reproducibility curve for lower time advances.

The difference between *Case 2* and *Case 3* in Fig. 11 is enlarged in Fig. 12. For this scenario, the difference due to the change of control penalty is at most just over 1 dB.

Now that it is established that no severe performance degradation of the noise reduction occurs in any of the three cases, the input signal power levels to the control loudspeakers for the three cases are compared using the total output power from the controller,

$$P = \lim_{t\to\infty} \frac{1}{t} \sum_{t} |u(t)|^2 = \frac{1}{2\pi} \sum_{\omega} |\mathcal{R}(e^{-j\omega})|^2,$$

when the feedforward signal $n(t)$ is white noise with unit power. Table II shows the powers of the input signals to each control loudspeaker for the three cases considered, as well as the total sum over all the loudspeakers, averaged over one second.[6] Also, the ratios of the total sums are presented. It is seen that reducing the numbers of control loudspeakers from 15 to 11 reduces the total input power by 24%. The input signal powers to the individual loudspeakers increased somewhat when removing four of the loudspeakers. Although the total sum over all the loudspeakers decreased, some of the signal power from the removed loudspeakers was redistributed over the remaining loudspeakers.

TABLE II
POWER OF SIGNALS TO THE CONTROL LOUDSPEAKERS FOR THREE DIFFERENT CONTROLLER DESIGNS

Speaker (midrange/subwoofer)	$\frac{1}{2\pi}\sum \lvert\boldsymbol{R}_1\rvert^2$	$\frac{1}{2\pi}\sum \lvert\boldsymbol{R}_2\rvert^2$	$\frac{1}{2\pi}\sum \lvert\boldsymbol{R}_3\rvert^2$
1, midrange	50.1	56.8	56.6
3, midrange	68.2	79.2	79.0
4, subwoofer	0.57	0.69	0.65
5, midrange	36.2	38.1	38.0
6, midrange	17.0	19.0	19.1
7, midrange	26.0	26.7	26.7
8, subwoofer	0.3	0.43	0.41
9, midrange	55.9	63.7	63.6
10, midrange	42.8	50.0	49.8
11, midrange	72.8	0	0
12, midrange	50.4	0	0
13, midrange	102.4	117.9	117.9
14, midrange	30.9	38.5	38.5
15, midrange	48.3	0	0
16, midrange	47.8	0	0
Total	649.6	491.2	490.1
$*/\sum \lvert\boldsymbol{R}_1\rvert^2$	1	0.756	0.755
$*/\sum \lvert\boldsymbol{R}_2\rvert^2$	-	1	0.998

Also penalizing the use of the hard-to-use input directions when using 11 control loudspeakers leaves the total input power unchanged as compared to *Case 2*. The change in individual input signal powers when going from the diagonal control signal penalty matrix to the more advanced is also insignificant in the

[6]The scaling of the power to the midrange loudspeakers is very different than that to the subwoofers. This is because the two loudspeaker types had different settings for their amplifiers (both are active loudspeakers). A better comparison would be to use the signal powers after amplification, however unfortunately these were not available.

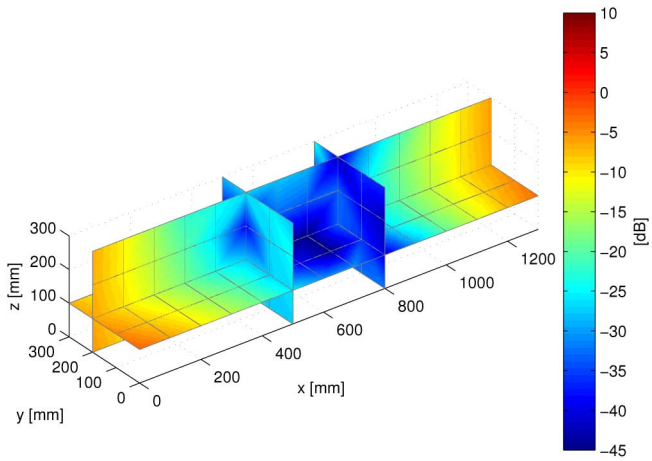

Fig. 13. The resulting attenuation in all the 244 measurement positions after control over Grid 1 for a 150 Hz feedforward noise signal. The sound field has been interpolated between the measurement positions to make interpretation easier.

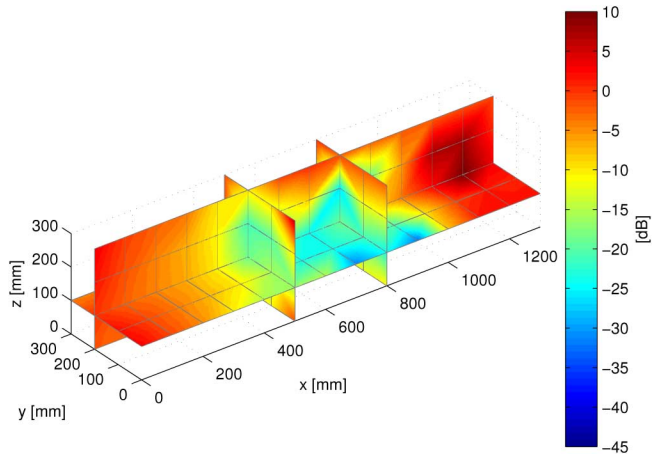

Fig. 14. The resulting attenuation in all the 244 measurement positions after control over Grid 1 for a 400 Hz feedforward noise signal. The sound field has been interpolated between the measurement positions to make interpretation easier.

investigated experimental setup. This indicates that the diagonal control signal penalty matrix is adequate in terms of control signal economy. Control strategies that use the hard-to-use input directions would need to generate large inputs to some combinations of loudspeakers. Therefore, already the use of a diagonal control penalty matrix will to a large extent prevent the controller from using the hard-to-use input directions. Using the more advanced control signal penalty matrix (22) therefore does not seem necessary unless there is a problem with ill-conditioning resulting from near linear dependence in the columns of $\boldsymbol{\mathcal{H}}(q^{-1})$.

This result also explains why the RMS average of the attenuation in Fig. 7 and Fig. 8 (obtained with a diagonal penalty matrix) was rather well predicted by the corresponding reproducibility curve in Fig. 6. The accuracy of that performance measure does by Section II-E rely on that the hard-to-use input directions are not used. This is indeed the case in the present example, also in *Case 2*, where the diagonal control penalty matrix was used.

G. Validation Outside of the Small Grid

It is of interest to examine how the sound field behaves outside the area or volume targeted for ANC, in particular to investigate to what extent noise amplification occurs outside of the control grid.

Simulations were performed, where the resulting sound field after control was calculated at all of the 244 measurement positions above the living room sofa. The controller design was made for Grid 1, using 11 control loudspeakers and a simple diagonal control signal penalty matrix $\boldsymbol{W}(q^{-1}) = \boldsymbol{W}_1(q^{-1})$. The remaining design choices were as discussed in Section III-B, namely d corresponding to 0.1 s and $\boldsymbol{V}(q^{-1}) = \mathbf{I}$. The results from simulations where the feedforward signal contains sinusoids at 150 Hz and 400 Hz are shown in Figs. 13 and 14 respectively.[7]

Figs. 13 and 14 show four slices through the volume of measurement positions above the living room sofa. The measurement positions used for the controller design, Grid 1, are located on the horizontal slice $z = 100$ mm, between the two vertical slices $x = 500$ mm and $x = 800$ mm. This grid is at a typical ear height of a listener. For 150 Hz, the zone of control extends outside the design grid in the z-direction. There is a considerable attenuation of the noise in the entire $0.3 \times 0.3 \times 0.3$ m volume around the 0.3×0.3 m Grid 1. At the sides, increasing or decreasing x, there is a degradation proportionate to the distance from Grid 1. This degradation seems fairly independent of the y-coordinate. At 400 Hz, a much faster degradation of performance outside of the design area as compared to 150 Hz is to be expected. This is due to the shorter wavelength and consequent increased complexity of the sound field. Fig. 14 shows the same general behavior as Fig. 13 but the degradation outside of Grid 1 is much faster, and the zone of control does not extend as far in the vertical z-direction as for 150 Hz.

IV. Discussion and Conclusion

The aim of this work has been to provide insights and tools that can be used to improve the controller design and the performance analysis for feedforward active noise control.

When the control path is known to be stationary, a model-based multi-point MMSE sound field control approach is an interesting and powerful alternative to the conventional adaptive control solutions. Feedforward control filter parameters can then be optimized in advance with respect to the performance in multiple positions that cover an extended area or volume. As shown in [17] and [18], this can significantly extend the area of

[7]In the figures, the sound field between the measurement positions has been interpolated using trilinear interpolation, in order to make the figures easier to read. To accurately reconstruct the sound field in between design points, more advanced interpolation methods are needed, see e.g. [21].

silence as compared to optimization in a few microphone positions, when using multiple loudspeakers. In this paper, the illustrative simulation case study based on measured room impulse responses results in an average attenuation of over 20 dB up to 350 Hz, and above 10 dB for frequencies up to 700 Hz over a 0.3×0.3 m area. In many situations, some parts of the system are time-invariant, while others (such as the properties of the reference signal $n(t)$) are nonstationary. It is therefore of interest to further develop this design into a partly fixed and partly adaptive design, in which some model parts are updated by on-line adaptation.

Regarding the *controller design*, we have evaluated the use of Linear Quadratic Gaussian multivariable feedforward filter design based on a polynomial equations approach. This method provides feedforward filters in the form of stable high-order IIR filters under a causality constraint. The choice of control penalty matrix has been investigated. Our preliminary conclusion is that a diagonal polynomial matrix (corresponding to the use of separate FIR penalty filters for each input signal component) provides good properties and little is gained by introducing the more complicated structures that have been investigated. With a reasonably frequency-weighted diagonal penalty matrix, large control excursions are avoided.

Regarding the *performance analysis*, we have shown the relation between a theoretical measure of sound field reproducibility and the obtained ANC performance when causality constraints are removed. We have separately characterized the performance penalty generated by a prescribed causality constraint. We have also shown how the effective rank of the control path can be used in a preliminary design phase. It may be used to identify possibilities to remove superfluous loudspeakers. It could be interesting to combine this with a scheme for finding the best locations out of a set of potential positions, such as the natural algorithms investigated in [27]. The effective rank and reproducibility tools reduce the computational burden when performing such preliminary investigations and are of use in many problem formulations that balance performance aspects against economic aspects.

APPENDIX

Consider the polynomial matrix Diophantine equation (10). Multiplying by $\boldsymbol{\beta}_*^{-1}(q^{-1})$ from the left, the equation becomes

$$q^{-d}\boldsymbol{\beta}_*^{-1}\boldsymbol{B}_*\boldsymbol{V}_*\boldsymbol{V}\boldsymbol{D} = \boldsymbol{Q} + q\boldsymbol{\beta}_*^{-1}\boldsymbol{L}_*\boldsymbol{F}\boldsymbol{E}. \tag{34}$$

Here, $\boldsymbol{Q}(q^{-1})$ is causal by definition, whereas the last term has impulse response coefficients for both positive and negative lags. The same is true for the left-hand side expression in (34). However, since $\boldsymbol{\beta}(q^{-1})$ is minimum phase, $\boldsymbol{\beta}^{-1}(q^{-1})$ is a stable system, so its impulse response will decay exponentially. This implies that the impulse response of $\boldsymbol{\beta}_*^{-1}(q)$ decays exponentially in forward (noncausal) time. Since both $\boldsymbol{B}(q^{-1})$ and $\boldsymbol{V}(q^{-1})$ are polynomial (FIR filter) matrices, the factor

$$\boldsymbol{\beta}_*^{-1}(q)\boldsymbol{B}_*(q)\boldsymbol{V}_*(q) = \sum_{i=0}^{\infty} N_i q^i \tag{35}$$

of the left-hand side of (34) will therefore have exponentially decaying impulse response coefficients matrices in forward time, $N_i \to 0$ when $i \to \infty$. This implies that when $d \to \infty$, the left-hand side of (34),

$$q^{-d}\boldsymbol{\beta}_*^{-1}\boldsymbol{B}_*\boldsymbol{V}_*\boldsymbol{V}\boldsymbol{D} = \left(\sum_{i=0}^{\infty} N_i q^{i-d}\right)\left(\sum_{j=0}^{n_V} V_j q^{-j}\right)\left(\sum_{k=0}^{n_D} D_k q^{-k}\right), \tag{36}$$

will approach a causal impulse response: all coefficients N_i for $i - d > 0$ vanish asymptotically. Since the last term in (34) has noncausal impulse response coefficients for any value of d, that term must therefore vanish when $d \to \infty$. Therefore we conclude that the indeterminate polynomial matrix $\boldsymbol{L}_*(q)$ in the Diophantine equation (10) approaches zero as $d \to \infty$. The polynomial matrix $\boldsymbol{Q}(q^{-1})$ therefore approaches the expression given by the left-hand side of (34) as $d \to \infty$, which gives (26) and (27).

REFERENCES

[1] S. J. Elliott and P. A. Nelson, "Multiple-point equalization in a room using adaptive digital filters," *J. Audio Eng. Soc.*, vol. 37, no. 11, pp. 899–907, Nov. 1989.

[2] L.-J. Brännmark, A. Bahne, and A. Ahlén, "Compensation of loudspeaker-room responses in a robust MIMO control framework," *IEEE Trans. Audio, Speech, Lang. Process.*, vol. 21, no. 6, pp. 1201–1216, Jun. 2013.

[3] E. Corteel, "Equalization in an extended area using multichannel equalization and wave field synthesis," *J. Audio Eng. Soc.*, vol. 54, no. 12, pp. 1140–1161, Dec. 2006.

[4] S. J. Elliott and P. A. Nelson, "Active noise control," *IEEE Signal Process. Mag.*, vol. 10, pp. 12–35, Oct. 1993.

[5] P. A. Nelson and S. J. Elliott, *Active Control of Sound*. San Diego, CA, USA: Academic, 1992.

[6] S. M. Kuo and D. R. Morgan, *Active Noise Control Systems - Algorithms and DSP Implementations*. New York, NY, USA: Wiley, 1996.

[7] S. M. Kuo and D. R. Morgan, "Active noise control: A tutorial review," *Proc. IEEE*, vol. 87, no. 6, pp. 943–973, Jun. 1999.

[8] H. Sano, T. Inoue, A. Takahashi, K. Terai, and Y. Nakamura, "Active control system for low-frequency road noise combined with an audio system," *IEEE Trans. Speech Audio Process.*, vol. 9, no. 7, pp. 755–763, Oct. 2001.

[9] S. J. Elliott and P. A. Nelson, "Multichannel active sound control using adaptive filtering," in *Proc. IEEE Int. Conf. Acoust., Speech, Signal Process. (ICASSP-88)*, 1988, vol. 5, pp. 2590–2593.

[10] T. J. Sutton, S. J. Elliott, A. M. McDonald, and T. J. Saunders, "Active control of road noise inside vehicles," *Noise Control Eng. J.*, vol. 42, pp. 137–147, Jul. 1994.

[11] A. J. Berkhout, D. de Vries, and P. Vogel, "Acoustic control by wave field synthesis," *J. Acoust. Soc. Amer.*, vol. 93, no. 5, pp. 2764–2778, May 1993.

[12] S. Spors, R. Rabenstein, and J. Ahrens, "The theory of wave field synthesis revisited," in *Proc. AES 124th Conv. Amsterdam, Audio Eng. Soc.*, May 2008, Preprint 7358.

[13] M. A. Poletti, "Three-dimensional surround sound systems based on spherical harmonics," *J. Audio Eng. Soc.*, vol. 53, no. 11, pp. 1004–1025, Nov. 2005.

[14] O. Kirkeby and P. A. Nelson, "Reproduction of plane wave sound fields," *J. Acoust. Soc. Amer.*, vol. 94, no. 5, pp. 2992–3000, Nov. 1993.

[15] Z. Wang and S. F. Wu, "Helmholtz equation - least-squares method for reconstructing the acoustic pressure field," *J. Acoust. Soc. Amer.*, vol. 102, no. 4, pp. 2020–2032, Oct. 1997.

[16] T. Betlehem and T. D. Abhayapala, "Theory and design of sound field reproduction in reverberant rooms," *J. Acoust. Soc. Amer.*, vol. 117, no. 4, pt. 1, pp. 2100–2111, Apr. 2005.

[17] A. Barkefors, S. Berthilsson, and M. Sternad, "Extending the area silenced by active noise control using multiple loudspeakers," in *Proc. IEEE Int. Conf. Acoust., Speech, Signal Process. (ICASSP-12)*, 2012, pp. 325–328.

[18] S. Berthilsson, A. Barkefors, and M. Sternad, "MIMO design of active noise controllers for car interiors: Extending the silenced region at higher frequencies," in *Proc. Amer. Control Conf. (ACC)*, Jun. 2012, pp. 6140–6147.

[19] A. Ahlén and M. Sternad, "Wiener filter design using polynomial equations," *IEEE Trans. Signal Process.*, vol. 39, no. 11, pp. 2387–2399, Nov. 1991.
[20] Y. Huang, J. Benesty, and J. Chen, *Acoustic MIMO Signal Processing*. New York, NY, USA: Springer, 2006.
[21] L.-J. Brännmark, "Robust sound field control for audio reproduction: A polynomial approach to discrete-time acoustic modeling and filter design," Ph.D. dissertation, Uppsala Univ., Uppsala, Sweden, 2011.
[22] L.-J. Brännmark and A. Ahlén, "Spatially robust audio compensation based on SIMO feedforward control," *IEEE Trans. Signal Process.*, vol. 57, no. 5, pp. 1689–1702, May 2009.
[23] M. Johansson, L.-J. Brännmark, A. Bahne, and M. Sternad, "Sound field control using a limited number of loudspeakers," in *Proc. AES 36th Int. Conf.: Automotive Audio*, Dearborn, MI, USA, 2009, AES.
[24] S. Berthilsson, A. Barkefors, L.-J. Brännmark, and M. Sternad, "Acoustical zone reproduction for car interiors using a MIMO MSE framework," in *Proc. AES 48th Int. Conf.: Automotive Audio*, Munich, Germany, Sep. 2012.
[25] O. Kirkeby, P. A. Nelson, H. Hamada, and F. Orduna-Bustamante, "Fast deconvolution of multichannel systems using regularization," *IEEE Trans. Speech Audio Process.*, vol. 6, no. 2, pp. 189–194, Mar. 1998.
[26] T. Betlehem and C. Withers, "Sound field reproduction with energy constraint on loudspeaker weights," *IEEE Trans. Audio, Speech, Lang. Process.*, vol. 20, no. 8, pp. 2388–2392, Nov. 2012.
[27] K. Baek and S. Elliott, "Natural algorithms for choosing source locations in active control systems," *J. Sound Vibr.*, vol. 186, no. 2, pp. 245–267, Sep. 1995.
[28] G. N. Lilis, D. Angelosante, and G. B. Giannakis, "Sound field reproduction using the lasso," *IEEE Trans. Audio, Speech, Lang. Process.*, vol. 18, no. 8, pp. 1902–1912, Nov. 2010.
[29] H. Khalilian, I. V. Bajic, and R. G. Vaughan, "Towards optimal loudspeaker placement for sound field reproduction," in *Proc. IEEE Int. Conf. Acoust., Speech, Signal Process.*, May 2013, pp. 321–325.
[30] T. Kailath, *Linear Systems*. Englewood Cliffs, NJ, USA: Prentice-Hall, 1980.
[31] Y. Haneda, S. Makino, and Y. Kaneda, "Common acoustical pole and zero modeling of room transfer functions," *IEEE Trans. Speech Audio Process.*, vol. 2, no. 2, pp. 320–328, Apr. 1994.
[32] T. Söderström and P. Stoica, *System Identification*. Hertfordshire, U.K.: Prentice-Hall, 1989.
[33] L. Ljung, *System Identification: Theory for the User*, 2nd ed. Upper Saddle River, NJ, USA: Prentice-Hall, 1999.
[34] O. Kirkeby, "Reproduction of acoustic fields," Ph.D. dissertation, Univ. of Southampton, U.K., 1995.
[35] B. D. O. Anderson and J. B. Moore, *Optimal Control. Linear Quadratic Methods*. Englewood Cliffs, NJ, USA: Prentice-Hall, 1989.
[36] M. Sternad and A. Ahlén, "LQ controller design and self-tuning control," in *Polynomial Methods in Optimal Control and Filtering*, K. Hunt, Ed. London, U.K.: Peter Peregrinus, 1993, pp. 56–92.
[37] K. Öhrn, A. Ahlén, and M. Sternad, "A probabilistic approach to multivariable robust filtering and open-loop control," *IEEE Trans. Autom. Control*, vol. 40, no. 3, pp. 405–418, Mar. 1995.
[38] L.-J. Brännmark, "Robust audio precompensation with probabilistic modeling of transfer function variability," in *Proc. IEEE Workshop Applicat. Signal Process. Audio Acoust. (WASPAA'09)*, New Paltz, NY, USA, Oct. 2009, pp. 193–196.
[39] K. J. Åström and B. Wittenmark, *Adaptive Control*, 2nd ed. New York, NY, USA: Dover, 2008.
[40] A. Barkefors, "Linear quadratic gaussian controllers for feedforward active noise control," Licentiate Thesis, University, Sweden, 2014.
[41] A. Papoulis, *Probability, Random Variables, and Stochastic Processes*, 3rd ed. Singapore: McGraw-Hill, 1991.
[42] J. M. Maciejowski, *Multivariable Feedback Design*. Wokingham, U.K.: Addison-Wesley, 1989.
[43] H. M. Jones, R. A. Kennedy, and T. D. Abhayapala, "On dimensionality of multipath fields: Spatial extent and richness," in *Proc. IEEE Int. Conf. Acoust., Speech, Signal Process. (ICASSP'02)*, Orlando, FL, USA, May 2002, pp. 2837–2840.
[44] R. A. Kennedy, P. Sadeghi, T. D. Abhayapala, and H. M. Jones, "Intrinsic limits of dimensionality and richness in random multipath fields," *IEEE Trans. Signal Process.*, vol. 55, no. 6, pp. 2542–2556, Jun. 2007.
[45] O. Roy and M. Vetterli, "The effective rank: A measure of effective dimensionality," in *Proc. 15th Eur. Signal Process. Conf. (EUSIPCO 07)*, Poznan, Poland, Sep. 2007, pp. 606–610.
[46] T. Betlehem and P. D. Teal, "A constrained optimization approach for multi-zone surround sound," in *Proc. IEEE ICASSP*, 2011, pp. 437–440.
[47] A. Barkefors, S. Berthilsson, and M. Sternad, "An investigation of a theoretical tool for predicting performance of an active noise control system," in *Poc. Int. Congr. Sound Vibr.*, Jul. 2012.

Annea Barkefors (S'12) received an M.Sc. degree in engineering physics from Uppsala University, Uppsala, Sweden, in 2010. She was with Uppsala, where she received a licentiate degree in electrical engineering with specialization in automatic control in 2014. Currently she is an industrial Ph.D. student in collaboration with Dirac Research, Uppsala, Sweden.

Her research interests are sound field control in general and active noise control in particular.

Mikael Sternad (S'83–M'86–SM'90) is professor in automatic control at Uppsala University in Sweden. He obtained his Ph.D. in automatic control in 1987 from the Institute of Technology at Uppsala University, Sweden.

One of his main research interests is signal processing applied to mobile broadband communication problems, such as channel prediction schemes for fast link adaptation, scheduling and coordinated multipoint transmission but also overall system aspects such as efficient MAC layer design. In this field, he has acted as project leader of the national 4G research project Wireless IP and the Swedish Research Council Framework project Dynamic Multipoint Transmission. He was engaged in the EU WINNER and Artist4G projects on 4G wireless systems and is at present active in the EU FP7 project METIS aiming at a 5G system proposal.

Another research interest is robust and adaptive MIMO feedforward control algorithms. These can be applied to wireless transmission (network MIMO, or CoMP), as well as well as to sound field control using multiple loudspeakers. He is co-founder and was chairman (2001-2005) of the company Dirac Research which is active in audio signal processing. He has published 6 book chapters, 34 journal papers, more than 110 conference papers and holds 10 patents.

Lars-Johan Brännmark was born in Luleå, Sweden, in 1974. He received the M.S. and Ph.D. degrees from Uppsala University in 2004 and 2011, respectively. He holds a Diploma in sound engineering from Piteå School of Music, Luleå University of Technology and he has also studied Electrical Engineering at Purdue University, Indiana, and musicology at Uppsala University. He has a professional background as a Sound Engineer at the Swedish National Radio and as a Research Engineer at Dirac Research AB. During 2011–2013 he was a Postdoctoral Researcher at the Department of Engineering Sciences, Uppsala University, and since 2011 he has held the position as Chief Scientist at Dirac Research AB. His research interests are in the field of signal processing for audio applications.